APL Materials

RESEARCH ARTICLE | APRIL 17 2024

Willis coupling in one-dimensional poroelastic laminates

J.-P. Groby ; M. R. Haberman

APL Mater. 12, 041120 (2024)
https://doi.org/10.1063/5.0194467

AIP Publishing

Willis coupling in one-dimensional poroelastic laminates

Cite as: APL Mater. 12, 041120 (2024); doi: 10.1063/5.0194467
Submitted: 27 December 2023 • Accepted: 31 March 2024 •
Published Online: 17 April 2024

J.-P. Groby[1,a] and M. R. Haberman[2]

AFFILIATIONS

[1] Laboratoire d'Acoustique de l'Université du Mans, LAUM - UMR 6613 CNRS, Le Mans Université, Avenue Olivier Messiaen, 72085 Le Mans Cedex 9, France
[2] Walker Department of Mechanical Engineering, The University of Texas at Austin, Austin, Texas 78712-1591, USA

Note: This paper is part of the Special Topic on New Frontiers in Acoustic and Elastic Metamaterials and Metasurfaces.
[a] **Author to whom correspondence should be addressed:** Jean-Philippe.Groby@univ-lemans.fr

ABSTRACT

We employ the Baker–Campbell–Hausdorff formula to derive closed-form expressions for the effective properties, including emergent Willis coupling, of a one-dimensional heterogeneous poroelastic medium consisting of a periodically repeating two-layer unit-cell. In contrast to the elastic and fluidic analogs, the Willis coupling of this periodic poroelastic medium *does not* vanish in the low-frequency limit. However, the effective wavenumber and impedance of this asymmetric lamellar material demonstrate symmetric reflection and absorption behavior that is indicative of symmetric structures in the low-frequency limit due to the effect of Darcy's law on the dynamic effective density, which is inversely proportional to frequency. These closed-form expressions are validated against results obtained by direct numerical evaluation. The scattering coefficients, particularly the two reflection coefficients for incidence from either side of a finite length asymmetric structure, are different at non-zero frequencies but still in the metamaterial limit and are correct when the Willis coupling is included. The results show that asymmetry in poroelastic layers results in direction-dependent absorption coefficients, one of which could be optimized based on layer properties and asymmetry factors. As a consequence, the frequency range of validity of these scattering coefficients is wider when the Willis coupling matrix is accounted for than in its absence. This work paves the way for better control of elastic and acoustic waves in multiphase materials by considering poroelastic behavior.

I. INTRODUCTION

Materials whose dynamic response is described by constitutive relations that couple the stress-strain behavior to the conservation of momentum expression have come to be known as "Willis materials" in reference to the seminal work by John Willis in his efforts to homogenize the dynamic response of heterogeneous elastic materials.[1–3] Since Willis' original work in the 1980s, the eponymous materials have received increased attention, particularly since their recent experimental demonstration.[4–6] The Willis coupling parameter is directional and couples the potential and kinetic energy in the conservation relations,[7] therefore enhancing the ability of materials with this coupling to control waves in (meta)materials compared to conventional materials that do not exhibit such coupling. Initially described in the context of elastodynamics,[1,8,9] Willis coupling has been explored in the context of waves in elastic beam structures,[6,10] airborne acoustic waves,[4,5,11] piezoelectric systems,[12] and water waves[13] and has been shown to enable direction-dependent and unidirectional absorption in acoustic[14,15] and flexural wave systems.[16] To the authors' knowledge, Willis coupling has not yet been considered in poroelastic systems, which have broad applicability in acoustic and elastic wave control. The present article aims to fill this gap by investigating one-dimensional (1D) acoustic wave phenomena in heterogeneous poroelastic media with subwavelength asymmetry.

Multilayered poroelastic materials are often used in transportation and building industries to reduce noise levels, where the layered structure can be designed to improve sound absorption.[17] The present study considers a simple poroelastic unit-cell composed of two poroelastic layers of infinite lateral extent. This minimalist

configuration has previously been considered to study bandgap formation in periodic poroelastic systems.[18] Although relying on two solid phases with an interpenetrating fluid phase (with the saturating fluid being the same in both layers in practice), the resulting response is different from what would be expected of three phase (or multiphase) materials[19,20] because the two solid phases are not mixed and are not connected to both unit-cell interfaces. Poroelastic materials possess two main features: (*i*) they support two compressional waves, a "fast" and "slow" wave, and one shear wave due to the interconnected bi-material frame-pore structure of these materials; and (*ii*) the propagation of these waves requires that one account for (thermo)-viscous losses, which originate from Darcy's law.[21–23] Due to the fact that we only consider normal incidence and isotropic materials, only two coupled compressional waves are anticipated for this configuration. The complex interaction between the wave predominantly carried by the solid phase and the fluid phases is evidenced in this work. The system is modeled using a transfer matrix approach by casting the dynamical equations of poroelasticity in matrix form and considering the case where the thickness of each layer is much less than the wavelength of propagating waves via the Baker–Campbell–Hausdorff (BCH) formula.[24–26] The resulting closed-form expressions provide relationships for the effective material properties that arise from the first- and second-order terms, which result in effective constitutive relations of the Willis form. The BCH formula is perfectly suited to our minimalist system, whose modeling relies on transfer matrices that only involve matrix exponentials. In addition, it avoids tedious calculations involving matrices of rank greater than two when Padé's approximation of the exponential matrix is employed.[27] The closed-form expression derived here highlights not only the strong coupling between displacements and stresses and their first-order spatial derivatives but also sheds further light on the problem of relative permeability of a two-phase flow[28–32] and Gedeon streaming in thermoacoustics.[33,34]

In this paper, we show that Willis coupling does not vanish at low frequency in the presence of viscous losses because of Darcy's law in each layer of the bi-layered structure. Nevertheless, asymmetry in acoustic reflection and absorption behavior vanishes in the quasi-static limit, consistent with expectations of scattering behavior in the long-wavelength limit. The closed-form expressions of the effective properties are validated numerically. The scattering coefficients of a finite thickness structure clearly demonstrate the need to consider Willis coupling to correctly model the direction-dependent reflection and absorption coefficients, as well as a widening of the bandwidth of model validity when Willis coupling is accounted for compared with coefficients based on the first-order homogenization theory.

II. CONSTITUTIVE RELATIONS OF POROELASTICITY

Consider the case of one-dimensional wave propagation in a poroelastic medium using the alternative formulation proposed by Biot in 1962.[23] Assuming an implicit time dependence $e^{-i\omega t}$, the pressure field in the fluid p, the total normal stress σ_{xx}, the elastic displacement u, and the relative displacement between the fluid and elastic frame $w = \phi(U-u)$, with ϕ representing the porosity and U representing the fluid displacement, all satisfy the following set of first order equations:

$$\begin{cases} \omega^2\tilde{\rho}w + \omega^2\rho_{\mathrm{f}}u = -\dfrac{\partial \tilde{P}}{\partial x}, \\ \omega^2\rho_{\mathrm{f}}w + \omega^2\rho u = -\dfrac{\partial \sigma_{xx}}{\partial x}, \\ \tilde{P} = M\dfrac{\partial w}{\partial x} + \alpha M\dfrac{\partial u}{\partial x}, \\ \sigma_{xx} = \alpha M\dfrac{\partial w}{\partial x} + \left(K_{\mathrm{G}} + \dfrac{4N}{3}\right)\dfrac{\partial u}{\partial x}. \end{cases} \tag{1}$$

In these relations, $\tilde{\rho}$ is a complex and frequency-dependent density arising from Darcy's law that accounts for viscous losses;[35] ρ_{f} is the density of the saturating fluid; $\rho = \phi\rho_{\mathrm{f}} + (1-\phi)\rho_{\mathrm{s}}$ is the volume averaged effective density of the poroelastic medium, with ρ_{s} representing the density of the elastic solid phase; M is an additional elastic parameter related to the coupling of relative fluid-frame motion to the local stress; α is an elastic coupling coefficient; K_{G} is the saturated (or "un-drained") bulk modulus; and N is the dry shear modulus. The expressions of these coefficients in terms of $\tilde{K}$ (the complex and frequency-dependent bulk modulus of the fluid phase that accounts for the thermal losses[36]), K_{b} (the bulk modulus of the bulk material), and K_{s} (the bulk modulus of the solid phase), as well as that of the complex and frequency-dependent density, $\tilde{\rho}$, are provided in Appendix A. Note that we have defined $\tilde{P} = -p$ to be consistent with the sign convention of normal stress.[37–39] This system of equations can be cast in the following matrix form:

$$\frac{\partial}{\partial x}\boldsymbol{W} = \begin{bmatrix} 0 & 0 & -\omega^2\tilde{\rho} & -\omega^2\rho_{\mathrm{f}} \\ 0 & 0 & -\omega^2\rho_{\mathrm{f}} & -\omega^2\rho \\ \tilde{C}_{\mathrm{f}} & -\alpha\tilde{C} & 0 & 0 \\ -\alpha\tilde{C} & \tilde{C} & 0 & 0 \end{bmatrix}\boldsymbol{W} = \begin{bmatrix} \boldsymbol{0} & -\omega^2\boldsymbol{\rho} \\ \boldsymbol{C} & \boldsymbol{0} \end{bmatrix}\boldsymbol{W} = \boldsymbol{A}\boldsymbol{W}, \tag{2}$$

where $\boldsymbol{W} = \{\tilde{P}, \sigma_{xx}, w, u\}^{\mathrm{T}}$ is the state vector; $\boldsymbol{0}$ is a 2×2 matrix, the elements of which are 0; $\boldsymbol{\rho}$ is a density matrix; $\boldsymbol{C}$ is the compliance matrix; and $\boldsymbol{A}$ is the propagator matrix. The compressibilities (i.e., compliances) $\tilde{C}_{\mathrm{f}} = (K_{\mathrm{G}} + \frac{4N}{3})/(M(K_{\mathrm{G}} + \frac{4N}{3}) - \alpha^2M^2)$ and $\tilde{C} = 1/((K_{\mathrm{G}} + \frac{4N}{3}) - \alpha^2M)$ are introduced for conciseness and clearly exhibit a strong coupling between the solid and the fluid phases. The compliance matrix was previously introduced[37–39] to ease the static homogenization of poroelastic medium. Using this formulation, $\tilde{C}$ reduces to $1/(K_{\mathrm{G}} + \frac{4N}{3})$ when the fluid phase vanishes, and $\tilde{C}_{\mathrm{f}}$ reduces to $1/M$ when the skeleton is motionless or vanishes. The solution of the system Eq. (2), which relates the state vector at $x = l$ to the state vector at $x = 0$ via the transfer matrix $\boldsymbol{T}_l$, is

$$\boldsymbol{W}(l) = \boldsymbol{T}_l\boldsymbol{W}(0) = \mathrm{expm}(\boldsymbol{A}l)\boldsymbol{W}(0), \tag{3}$$

where $\mathrm{expm}(\boldsymbol{A}l)$ is the matrix exponential of $\boldsymbol{A}l$.

III. THE EFFECTIVE PROPERTIES OF A TWO-LAYER LAMELLA

We now assume the two-layer poroelastic lamellar material depicted in Fig. 1(a). The lamellar system consists of the d-periodic

repetition of a layer of thickness l_1 with a propagator matrix $\boldsymbol{A}_1$ and a layer of thickness l_2 with a propagator matrix $\boldsymbol{A}_2$, where $d = l_1 + l_2$. The state vectors at both sides of the unit cell are related via the total transfer matrix $\boldsymbol{T}_{\mathrm{d}}$, which is the multiplication of the transfer matrices of these two layers, i.e., $\boldsymbol{T}_{\mathrm{d}} = \mathrm{expm}(\boldsymbol{A}_2 l_2)\mathrm{expm}(\boldsymbol{A}_1 l_1)$. This total transfer matrix is then simply $\mathrm{expm}(\boldsymbol{A}_{\mathrm{e}} d)$, where $\boldsymbol{A}_{\mathrm{e}}$ is the effective propagation matrix of this two-layer lamellar unit-cell that contains the effective properties. As a result, the two-layer lamellar (composite) poroelastic material must yield an effective medium where the field variables satisfy the following first-order matrix propagator equation:

$$\frac{\partial}{\partial x}\boldsymbol{W} = \boldsymbol{A}_e \boldsymbol{W}. \tag{4}$$

We note that the state vector in the effective medium, $\boldsymbol{W} = \{\tilde{P}, \sigma_{xx}, w, u\}^{\mathrm{T}}$, is composed of the same field variables as the individual layers, and therefore, the propagation in the effective medium is that in a poroelastic medium, although it is shown below that the effective properties may differ from those of a conventional poroelastic medium if the layered structure is asymmetric.

The resulting identity for the propagator matrix of the two-layer system is then

$$\mathrm{expm}(\boldsymbol{A}_e d) = \mathrm{expm}(\boldsymbol{A}_2 l_2)\mathrm{expm}(\boldsymbol{A}_1 l_1), \tag{5}$$

the solution of which is provided by the Baker–Campbell–Hausdorff (BCH) formula.[24,25] The lowest order terms of this series are

$$\boldsymbol{A}_e d = \boldsymbol{A}_2 l_2 + \boldsymbol{A}_1 l_1 + \frac{1}{2}[\boldsymbol{A}_2 l_2, \boldsymbol{A}_1 l_1] + \cdots \tag{6}$$

where $[\boldsymbol{A}_2 l_2, \boldsymbol{A}_1 l_1] = \boldsymbol{A}_2 l_2 \boldsymbol{A}_1 l_1 - \boldsymbol{A}_1 l_1 \boldsymbol{A}_2 l_2$. The first term, $\boldsymbol{A}_2 l_2 + \boldsymbol{A}_1 l_1$, provides first-order homogenization effective properties, while the second term, $[\boldsymbol{A}_2 l_2, \boldsymbol{A}_1 l_1]/2$, provides the additional second-order terms. These terms are only non-zero if $\boldsymbol{A}_2 l_2 \boldsymbol{A}_1 l_1 \neq \boldsymbol{A}_1 l_1 \boldsymbol{A}_2 l_2$ and will be shown to be indicative of non-zero Willis coupling of the effective poroelastic medium. Keeping terms in second order in the expansion of the BCH formula and writing $\boldsymbol{A}_e$ in matrix form yields

$$\boldsymbol{A}_e \approx \begin{bmatrix} \boldsymbol{\chi}_e & -\omega^2 \boldsymbol{\rho}_e \\ \boldsymbol{C}_e & -\boldsymbol{\chi}_e^T \end{bmatrix}, \tag{7}$$

with

$$\boldsymbol{\rho}_e = \begin{bmatrix} \left(\frac{\tilde{\rho}_1 l_1 + \tilde{\rho}_2 l_2}{d}\right) & \left(\frac{\rho_{\mathrm{f}_1} l_1 + \rho_{\mathrm{f}_2} l_2}{d}\right) \\ \left(\frac{\rho_{\mathrm{f}_1} l_1 + \rho_{\mathrm{f}_2} l_2}{d}\right) & \left(\frac{\rho_1 l_1 + \rho_2 l_2}{d}\right) \end{bmatrix}, \qquad \boldsymbol{C}_e = \begin{bmatrix} \frac{\tilde{C}_{\mathrm{f}_1} l_1 + \tilde{C}_{\mathrm{f}_2} l_2}{d} & -\frac{\alpha_1 \tilde{C}_1 l_1 + \alpha_2 \tilde{C}_2 l_2}{d} \\ -\frac{\alpha_1 \tilde{C}_1 l_1 + \alpha_2 \tilde{C}_2 l_2}{d} & \frac{\tilde{C}_1 l_1 + \tilde{C}_2 l_2}{d} \end{bmatrix},$$
$$\boldsymbol{\chi}_e = \frac{\omega^2 l_1 l_2}{2d} \begin{bmatrix} \tilde{\rho}_1 \tilde{C}_{\mathrm{f}_2} - \tilde{\rho}_2 \tilde{C}_{\mathrm{f}_1} + \rho_{\mathrm{f}_2} \alpha_1 \tilde{C}_1 - \rho_{\mathrm{f}_1} \alpha_2 \tilde{C}_2 & \tilde{\rho}_2 \alpha_1 \tilde{C}_1 - \tilde{\rho}_1 \alpha_2 \tilde{C}_2 + \rho_{\mathrm{f}_1} \tilde{C}_2 - \rho_{\mathrm{f}_2} \tilde{C}_1 \\ \rho_2 \alpha_1 \tilde{C}_1 - \rho_1 \alpha_2 \tilde{C}_2 + \rho_{\mathrm{f}_1} \tilde{C}_{\mathrm{f}_2} - \rho_{\mathrm{f}_2} \tilde{C}_{\mathrm{f}_1} & \rho_{\mathrm{f}_2} \alpha_1 \tilde{C}_1 - \rho_{\mathrm{f}_1} \alpha_2 \tilde{C}_2 + \rho_1 \tilde{C}_2 - \rho_2 \tilde{C}_1 \end{bmatrix}, \tag{8}$$

where the two layers are assumed to be saturated by different fluids of respective densities ρ_{f_1} and ρ_{f_2}. This is impossible, in practice, without introducing an impermeable layer between the layers, and we therefore only consider the case $\rho_{\mathrm{f}_1} = \rho_{\mathrm{f}_2} = \rho_{\mathrm{f}}$. For this case, the leading order effective properties are the average values of the corresponding properties for a periodic two-layer poroelastic medium, that is

$$\tilde{C}_{\mathrm{fe}} = \frac{\tilde{C}_{\mathrm{f}_1} l_1 + \tilde{C}_{\mathrm{f}_2} l_2}{d}, \quad \alpha_e \tilde{C}_e = \frac{\alpha_1 \tilde{C}_1 l_1 + \alpha_2 \tilde{C}_2 l_2}{d}, \quad \tilde{C}_e = \frac{\tilde{C}_1 l_1 + \tilde{C}_2 l_2}{d},$$
$$\tilde{\rho}_e = \frac{\tilde{\rho}_1 l_1 + \tilde{\rho}_2 l_2}{d}, \quad \rho_{\mathrm{fe}} = \frac{\rho_{\mathrm{f}_1} l_1 + \rho_{\mathrm{f}_2} l_2}{d} = \rho_{\mathrm{f}} \quad \text{and} \quad \rho_e = \frac{\rho_1 l_1 + \rho_2 l_2}{d}. \tag{9}$$

Note that calculations only involving these first-order homogenized effective parameters, i.e., in the absence of asymmetry in the second order expansion of the BCH formula, which can be found throughout the literature (cf. Berryman[37]), are denoted by the superscript H in what follows. In practice, $\alpha_1 = \alpha_2 = 1$, when the poroelastic materials are saturated by a light fluid such as the air (see Appendix A), which yields $\alpha_e = \alpha_e \tilde{C}_e / \tilde{C}_e = 1$. The elements of the stiffness matrix, $\alpha_e M_e$, M_e, and $K_{\mathrm{G}e} + 4N_e/3$, representing the coupling and elastic moduli of the poroelastic medium, can be obtained by simply inverting the effective compliance matrix $\boldsymbol{C}_e$,

$$\boldsymbol{C}_e^{-1} = \begin{bmatrix} M_e & \alpha_e M_e \\ \alpha_e M_e & K_{\mathrm{G}e} + \frac{4N_e}{3} \end{bmatrix} = \frac{1}{\tilde{C}_{\mathrm{fe}} \tilde{C}_e - \alpha_e^2 \tilde{C}_e^2} \begin{bmatrix} \tilde{C}_e & \alpha_e \tilde{C}_e \\ \alpha_e \tilde{C}_e & \tilde{C}_{\mathrm{fe}} \end{bmatrix}, \tag{10}$$

which again clearly exhibits strong coupling between the elastic and fluid phases of both layers.

In the second order, the BCH formula directly provides two 2×2 diagonal matrices, $\boldsymbol{\chi}_e$ and $-\boldsymbol{\chi}_e^T$, where the fact that the lower diagonal is the negative transpose of the upper diagonal is a consequence of reciprocity. In addition, note that this is due to the use of $\tilde{P} = -p$ instead of p to represent the state variable for pressure. As a result, $\tilde{P}$ has the same sign as normal stress, rather than the usual definition of pressure. If written with p, the off-diagonal terms of these two matrices are swapped (related to the transpose) but not of opposite signs. The elements of $\boldsymbol{\chi}_e$ are differences in mass density and compressibility products alternated between the two different layers in a similar way as was previously shown for asymmetric layered structures.[26,40] Furthermore, due to poroelasticity, they are also functions of the contrast of the product of the poroelastic coupling factors, α_i, and combinations of mass density and compressibility.

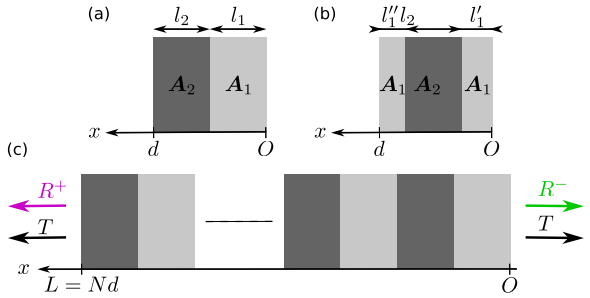

FIG. 1. Sketch of the two-layer poroelastic unit-cell (a), of another, but identical, two-layer poroelastic unit-cell comprising three layers (b), and of the scattering problem (b).

These additional terms arise due to the strong coupling between the elastic and fluid phases in the poroelastic layers. As suggested in Refs. 7 and 9, these two matrices may be divided by $-\mathrm{i}\omega$, i.e., $\boldsymbol{\psi}_e = \boldsymbol{\chi}_e/(-\mathrm{i}\omega)$, to make the time derivatives $\dot{u}$ and $\dot{w}$ of u and w, i.e., the elastic material velocity and fluid-elastic relative velocity, appear. We introduce the normal strain vector $\boldsymbol{\varepsilon} = \partial \boldsymbol{u}/\partial x$ with $\boldsymbol{u} = \{w, u\}^T$, which is composed of the elastic displacement and the relative displacement between the fluid and the elastic frame, such that the associated velocity vector is given by $\boldsymbol{v} = \dot{\boldsymbol{u}}$. We then define the stress vector $\boldsymbol{\sigma} = \{\tilde{P}, \sigma_{xx}\}^T$, which is composed of the negative of the pressure and the total normal stress, and introduce $\boldsymbol{\pi}$ as the momentum density such that $\dot{\boldsymbol{\pi}} = \partial \boldsymbol{\sigma}/\partial x$. Equations (4) and (7) take the form (see Appendix B)

$$\begin{cases} \boldsymbol{\sigma} = \boldsymbol{C}_e^{-1}\boldsymbol{\varepsilon} + \boldsymbol{S}_e\boldsymbol{v}, \\ \boldsymbol{\pi} = \boldsymbol{S}_e^T\boldsymbol{\varepsilon} + \boldsymbol{\rho}_e\boldsymbol{v}, \end{cases} \tag{11}$$

where $\boldsymbol{S}_e = \boldsymbol{\psi}_e\boldsymbol{C}_e^{-1}$ is the Willis coupling as introduced in the original works of Willis.[1–3]

This form is assumed causal,[7] and it becomes clear that the elements of $\boldsymbol{\psi}_e$ are linear functions of the frequency in the absence of losses [see Eq. (8)] and, thus, should vanish at low frequency. In other words, an asymmetric system effectively behaves as a symmetric system at low frequency. The viscothermal losses make the story different when poroelastic/porous materials are considered. For example, the low frequency limit of the effective density of the fluid phase reads as $i\eta/\omega\kappa_0$, where η is the dynamic viscosity and κ_0 is the viscous permeability, due to Darcy's law (see Appendix C). One may, therefore, anticipate that some elements of the Willis coupling matrix $\boldsymbol{\psi}_e$ will tend to a constant, non-zero value at low frequency as $\omega \to 0$, which differs from Willis coupling coefficients in purely acoustic and elastic media.[7,8,40]

To investigate this unique response of asymmetric porous media further, let us assume that the skeletons of the two poroelastic media are motionless. The relative velocity between fluid and elastic phases, $\dot{w}$, then reduces to the volume flux of the fluid phase $\mathscr{V} = \phi\dot{U}$, and the state vector reduces to $\boldsymbol{W}^{\mathrm{ef}} = \langle p, \mathscr{V}\rangle$, where the exponent $^{\mathrm{ef}}$ refers to equivalent fluid. In this limit, the constitutive equations become [see Appendix D and Eq. (4)]

$$\frac{\partial}{\partial x}\boldsymbol{W}^{\mathrm{ef}} = \mathrm{i}\omega\begin{bmatrix} -\psi_e^{\mathrm{ef}} & \tilde{\rho}_e^{\mathrm{ef}} \\ \tilde{C}_{\mathrm{fe}}^{\mathrm{ef}} & \psi_e^{\mathrm{ef}} \end{bmatrix}\boldsymbol{W}^{\mathrm{ef}} = \boldsymbol{A}_{\mathrm{e}}^{\mathrm{ef}}\boldsymbol{W}^{\mathrm{ef}}, \tag{12}$$

with $\psi_e^{\mathrm{ef}} = \mathrm{i}\omega l_1 l_2\left(\tilde{\rho}_1\tilde{C}_{\mathrm{f}2} - \tilde{\rho}_2\tilde{C}_{\mathrm{f}1}\right)/d$, $\tilde{\rho}_e^{\mathrm{ef}} = (\tilde{\rho}_1 l_1 + \tilde{\rho}_2 l2)/d$, and $\tilde{C}_{\mathrm{fe}}^{\mathrm{ef}} = \left(\tilde{C}_{\mathrm{f}1}l_1 + \tilde{C}_{\mathrm{f}2}l2\right)/d$. These expressions are derived from the expressions of the terms $\boldsymbol{A}_{\mathrm{e}}(1,1)$, $\boldsymbol{A}_{\mathrm{e}}(1,3)$, and $\boldsymbol{A}_{\mathrm{e}}(3,1)$ in Eq. (7) and are found in accordance with those found in Refs. 26 and 40. The low-frequency limit of these expressions reads as

$$\begin{aligned} \lim_{\omega\to 0}\psi_e^{\mathrm{ef}} &= \frac{-l_1 l_2\eta}{dP_0}\left(\frac{\phi_2}{\kappa_{01}} - \frac{\phi_1}{\kappa_{02}}\right), \\ \lim_{\omega\to 0}\tilde{\rho}_e^{\mathrm{ef}} &= \frac{\mathrm{i}\eta}{d\omega}\left(\frac{l_1}{\kappa_{01}} + \frac{l_2}{\kappa_{02}}\right), \\ \lim_{\omega\to 0}\tilde{C}_{\mathrm{fe}}^{\mathrm{ef}} &= \frac{1}{dP_0}(\phi_1 l_1 + \phi_2 l_2), \end{aligned} \tag{13}$$

where ϕ_j and κ_{0j} represent the porosity and viscous permeability of the jth layer, and P_0 is the ambient pressure. Notably, the low-frequency limit of ψ_e^{ef} is a non-zero real-valued constant, implying that the Willis coupling does not vanish. Nevertheless, the wavenumber $k_e^{\mathrm{ef}} = \omega\sqrt{\tilde{\rho}_e^{\mathrm{ef}}\tilde{C}_{\mathrm{fe}}^{\mathrm{ef}} + \left(\psi_e^{\mathrm{ef}}\right)^2}$ approaches $k_e^H \approx \omega\sqrt{\tilde{\rho}_e^{\mathrm{ef}}\tilde{C}_{\mathrm{fe}}^{\mathrm{ef}}}$ as $\omega \to 0$, and the characteristic impedance $Z_e^{\pm} = \tilde{\rho}_e^{\mathrm{ef}}/\left(\sqrt{\tilde{\rho}_e^{\mathrm{ef}}\tilde{C}_{\mathrm{fe}}^{\mathrm{ef}} + \left(\psi_e^{\mathrm{ef}}\right)^2} \mp \psi_e^{\mathrm{ef}}\right)$ approaches $Z_e^H = Z_e^+ = Z_e^- \approx \sqrt{\tilde{\rho}_e^{\mathrm{ef}}/\tilde{C}_{\mathrm{fe}}^{\mathrm{ef}}}$ in the same low frequency limit. This occurs because the product $\tilde{\rho}_e^{\mathrm{ef}}\tilde{C}_{fe}^{\mathrm{ef}} \propto \omega^{-1}$ while ψ_e^{ef} approaches a constant value in the low frequency limit, as shown in Eq. (13). This intriguing result shows that asymmetric laminates of poroelastic materials that have viscothermal losses will demonstrate behavior indicative of a symmetric system in the low frequency/long wavelength limit, despite the fact that the Willis coupling parameter does not vanish as $\omega \to 0$. This result, together with the approach proposed by Cacheux *et al.*,[31] should make it possible to extend Darcy's law to two-phase flows. The existence of a non-vanishing Willis coupling term in the low frequency limit implies that time-varying flow induces not only a pressure gradient as described by the conservation of momentum in a conventional material, but that there is an additional contribution to the pressure gradient that arises due to a temporal variation of the local pressure. This implies that time-varying pressure will lead to non-uniform strain fields. This strain gradient due to temporal variation in pressure leads to a gradient of the flow in addition to the volume change associated with the pressure-volume strain relation. In other words, an externally imposed spatially uniform but time-varying pressure field leads to a directional, time-varying volume flux. This first term has an impact on Darcy's law.

More generally, the non-vanishing Willis coupling terms in a poroelastic medium with a moving skeleton imply that time-varying flow will contribute to changes in momentum as with a conventional material, but also that it will induce gradients in the fluid pressure and elastic normal stress. In turn, the spatial derivatives of relative displacement and solid displacement are proportional to the relative velocity between the fluid and the elastic frame in the case of an asymmetric poroelastic lamina. In other words, stress induces

a spatial variation of the fluid and solid displacements in the presence of asymmetric permeability, which in-turn leads to flow whose direction depends on the microscale asymmetry.

To provide a complete analysis of this system for the case of an infinitely repeating bi-layer material, we assume that the unit-cell of the two-layer poroelastic lamellar material is translated along the x-axis as shown in Fig. 1(b). This lamellar system is identical to that previously analyzed from a bulk point of view. Nevertheless, the modification of the choice of unit cell yields a d-periodic repetition of two layers of thicknesses l_1' and l_1'' such that $l_1 = l_1' + l_1''$ with a propagator matrix $\boldsymbol{A}_1$ located on both sides of a layer of thickness l_2 with a propagator matrix $\boldsymbol{A}_2$, where $d = l_1 + l_2$. The effective properties of this specific $N = 3$-layer system (see Appendix E) are those in Eq. (9) at the first-order and

$$\boldsymbol{\chi}_e = \frac{\omega^2 l_2\left(l_1' - l_1''\right)}{2d}\begin{bmatrix} \tilde{\rho}_1\bar{C}_{\mathrm{f}_2} - \tilde{\rho}_2\bar{C}_{\mathrm{f}_1} + \rho_{\mathrm{f}_2}\alpha_1\bar{C}_1 - \rho_{\mathrm{f}_1}\alpha_2\bar{C}_2 & \tilde{\rho}_2\alpha_1\bar{C}_1 - \tilde{\rho}_1\alpha_2\bar{C}_2 + \rho_{\mathrm{f}_1}\bar{C}_2 - \rho_{\mathrm{f}_2}\bar{C}_1 \\ \rho_2\alpha_1\bar{C}_1 - \rho_1\alpha_2\bar{C}_2 + \rho_{\mathrm{f}_1}\bar{C}_{\mathrm{f}_2} - \rho_{\mathrm{f}_2}\bar{C}_{\mathrm{f}_1} & \rho_{\mathrm{f}_2}\alpha_1\bar{C}_1 - \rho_{\mathrm{f}_1}\alpha_2\bar{C}_2 + \rho_1\bar{C}_2 - \rho_2\bar{C}_1 \end{bmatrix}. \tag{14}$$

at the second order. The Willis coupling is, therefore, a clear marker of the asymmetry of the unit cell. It is maximum when either $l_1' = 0$ or $l_1'' = 0$ and vanishes for a symmetric unit-cell, i.e., when $l_1' = l_1'' = l_1/2$. When the unit-cell becomes symmetric, the first-order homogenization becomes also valid at the second order. The calculations denoted by the superscript H in what follows thus correspond to this case at the second order. This asymmetry is clearly exhibited when the scattering coefficients of a finite depth structure are calculated.

IV. RESULTS AND DISCUSSION

Consider a poroelastic laminate structure composed of two air-saturated poroelastic layers. The air is represented with the usual properties: mass density $\rho_{\mathrm{f}} = 1.213\ \mathrm{kg\cdot m^{-3}}$, adiabatic constant $\gamma = 1.4$, dynamic viscosity $\eta = 1.839 \times 10^{-5}$ Pa · s, Prandtl number of Pr = 0.71, and adiabatic bulk modulus of γP_0, where the atmospheric pressure is $P_0 = 1.013 \times 10^5$ Pa. The parameters of the two poroelastic layers are reported in Table I and are adapted from Ref. [41]. The layer thicknesses are $l_1 = l_2 = 1$ cm, such that $d = l_1 + l_2 = 2$ cm. Figure 2 depicts the effective parameters. The effective properties as calculated from Eqs. (8) and (9) are compared to those as numerically calculated from $\mathrm{logm}(\mathrm{expm}(\boldsymbol{A}_2 l_2)\mathrm{expm}(\boldsymbol{A}_1 l_1)) = A_e^{\mathrm{num}} d$, where $\mathrm{logm}(\boldsymbol{B})$ is the matrix logarithm of $\boldsymbol{B}$. The closed-form expressions of the effective parameters are in excellent agreement with those evaluated numerically up to ≈800 Hz. The real parts of both $\psi_e(1,1)$ and $\psi_e(1,2)$ do not vanish at low frequency and clearly possess a finite value. These two effective parameters involve the complex and frequency dependent densities in the fluid phase; see Eq. (8). The other two elements of the Willis coupling matrix, which only depend on the densities of the saturating fluid and of the effective poroelastic medium, vanish. This clearly shows that Willis coupling does not vanish when viscothermal losses are present. We note that around 1000 Hz, most of the closed form expression effective properties strongly deviate from those that have been evaluated numerically, most notably the compressibilities and the elements of the Willis coupling matrix. Critically, we note that the real part of the compliance $\bar{C}_e^{\mathrm{num}}$ changes sign, as does the imaginary part of the Willis coupling elements. The change in sign of the imaginary part of the Willis coupling is not permitted by passivity,[40] and thus, the effective properties are no longer valid. This is primarily due to the effective properties of the fluid phase in the poroelastic model. Of particular interest is the fact that the effective elastic coupling coefficient α_e deviates from 1 around this frequency and becomes a complex parameter, indicating that assumptions of the homogenization model are no longer valid beyond this limit.

The invalidity of the effective properties is evidenced by the dispersion relation depicted in Fig. 3(a). The real part of the normalized effective wavenumber in the fluid phase is larger than 0.5 for frequencies larger than ≈800 Hz in the case considered here, as evidenced by the gray region. In contrast, the real part of the normalized effective wavenumber in the solid phase is still much smaller than 0.5 and, thus, much smaller than that of the fluid phase. This shows that homogenization involving poroelastic material should provide valid expressions both for the solid and the fluid phases at the same time, although both are as strongly connected as one would anticipate due to the existence of poroelastic coupling. Figures 3(b)–3(d) depict the scattering coefficients (the transmission and the reflection coefficients for plane waves propagating in the $+x$ or $-x$ directions) of a finite layered structure composed of 10 bi-phase unit-cells, i.e., $L = 10d$, excited by an acoustic wave at normal incidence, as

TABLE I. Properties of the poroelastic media (adapted from Ref. [41]).

	ϕ	τ_∞	λ (μm)	λ' (μm)	κ_0 (m^2)	κ_0' (m^2)	$K_{\mathrm{b}}(1+\mathrm{i}\zeta)$ (kPa)	ν	ρ_{s}
M1	0.95	1.1	15	45	4.3786×10^{-10}	5.2543×10^{-10}	445.13 − i22.256	0.24	2520
M2	0.96	2.2	110	352	2.0433×10^{-9}	2.4520×10^{-9}	83.448 − i4.1724	0.21	925

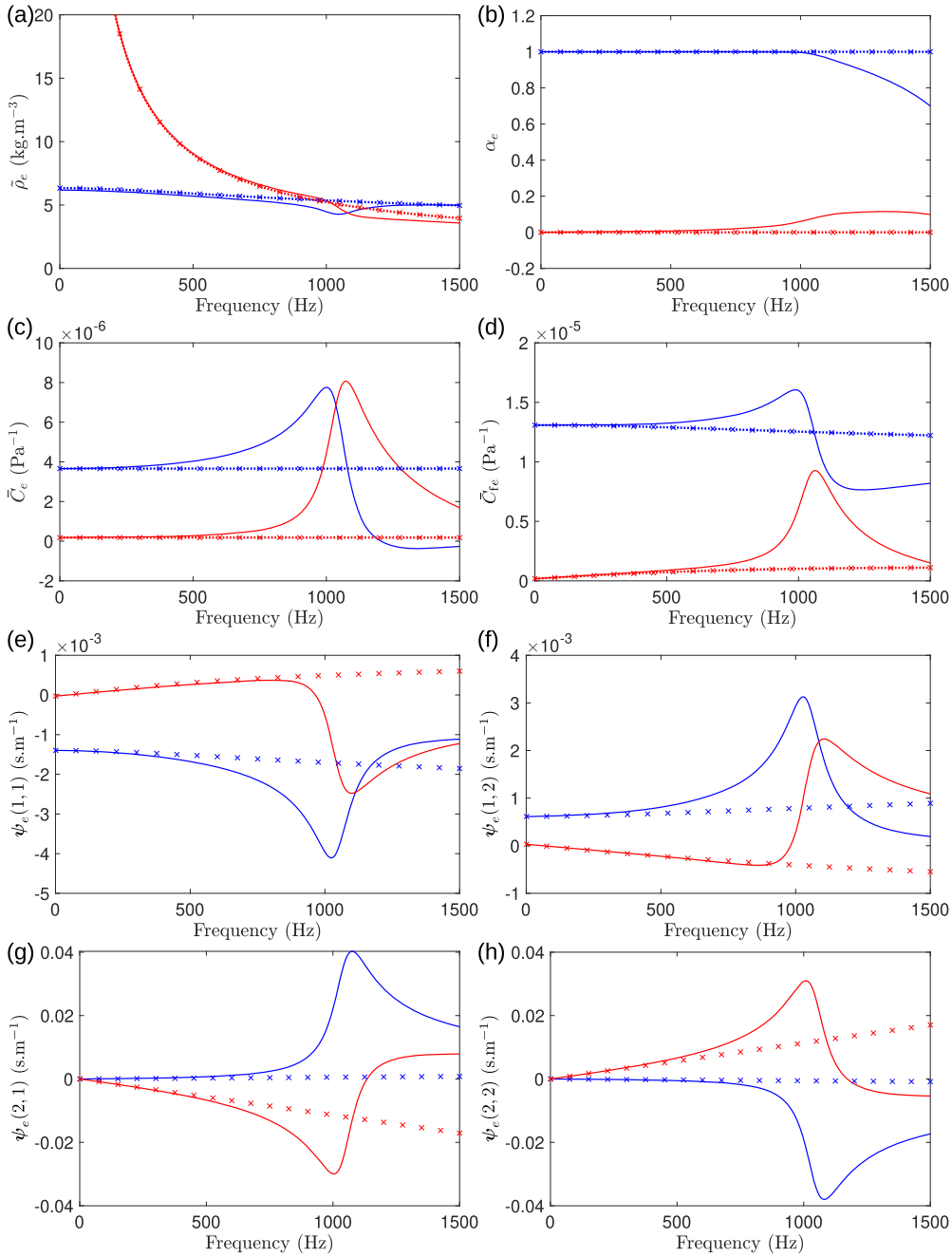

FIG. 2. Effective density $\tilde{\rho}_e$ (a), elastic coupling parameter α_e (b), compressibilities $\bar{C}_e$ (c), and $\bar{C}_{fe}$ (d), as well as the four Willis coupling parameters $\psi_e(1,1)$ (e), $\psi_e(1,2)$ (f), $\psi_e(2,1)$ (g), and $\psi_e(2,2)$ (h), are depicted in the function of the frequency. Blue and red curves and symbols represent the real and imaginary parts, respectively, of the effective parameter. The solid curves correspond to the effective parameters evaluated numerically, the dotted curves (a)–(d) correspond to the first-order homogenization parameters, and the crosses correspond to the homogenized properties obtained by including terms up to second-order in the BCH formula.

depicted in Fig. 1(c). The shaded regions indicate that second-order homogenization is questionable in these frequency ranges. These coefficients are evaluated following Appendix F. The scattering coefficients, as calculated numerically and as calculated from the second-order homogenization parameter procedure, are again in good agreement up to ≈800 Hz. As shown by Figs. 3(c)–3(e), both reflection coefficients R^+ and R^- are identical at low frequency and become different at higher frequency, but within the limits of valid-

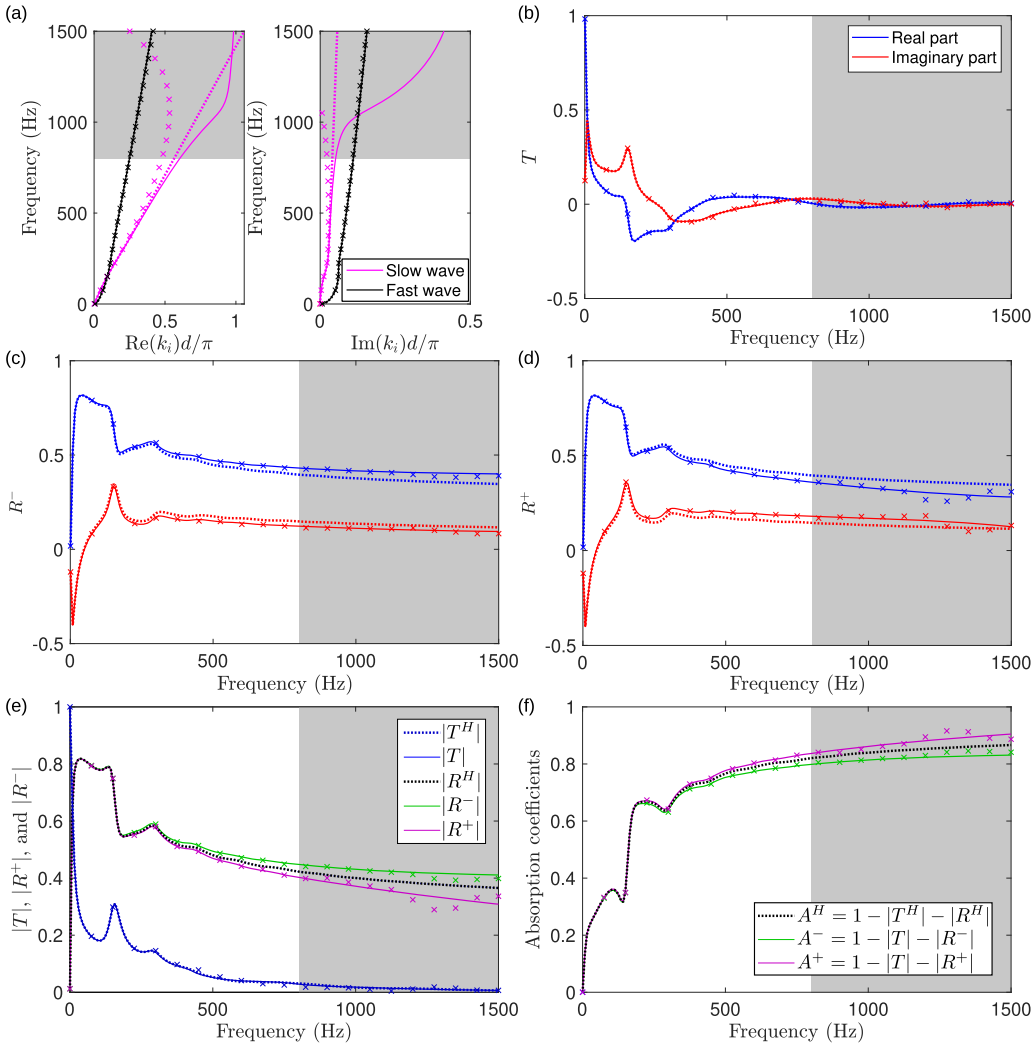

FIG. 3. (a) Dispersion relations for the fast and slow waves for a $L = 10d$ thick poroelastic layered structure whose properties provided in Table I. Scattering coefficients provided in (b)–(d) depict the transmission coefficient and the two reflection coefficients for incidence from the right and left, respectively. Corresponding absolute values of the scattering coefficients (e) and absorption coefficients (f) from the right and left, respectively. The solid curves correspond to the scattering coefficients evaluated numerically, the dotted curves (a)–(f) correspond to those calculated when only the first-order homogenization parameters are accounted for, and the crosses correspond to those calculated when the second-order homogenization parameters are included.

ity of the model due to layering asymmetry, which is a hallmark of Willis coupling.[5,14] This leads to direction-dependent absorption coefficients at high frequencies, as evidenced in Fig. 3(f). Importantly, the scattering coefficients calculated using only the first-order homogenization parameters exhibit identical reflection coefficients regardless of the frequency range. This illustrates numerous important points: (*i*) the need to take Willis coupling into account, (*ii*) that asymmetric poroelastic structures behave like symmetric structures in the long-wavelength limit despite the fact that some elements of the Willis coupling matrix do not vanish when viscothermal losses are present, and (*iii*) an extension of the frequency range over which calculations are valid when the Willis coupling matrix is taken into account compared to calculations carried out in its absence.

V. CONCLUSION

The effective properties of a two-layer poroelastic unit-cell are derived via the Baker–Campbell–Hausdorff formula. The compliance matrix is more suitable than the stiffness matrix to derive the closed-form expressions of the effective properties. The first term of the Baker–Campbell–Hausdorff formula provides the effective

density and compressibility in agreement with previous studies, while the second term exactly provides the elements of the Willis coupling matrix. The latter satisfies the reciprocity condition when the opposite sign of the pressure is considered to be consistent with the stress tensor. We show that the elements of the Willis coupling matrix involving the complex and frequency dependent densities of the fluid phases do not vanish at low frequency and possess a real value at the static limit. This real value depends on the porosity and permeability of the effective fluids the two-layer lamella is composed of and originates from Darcy's law. This offers a new perspective on relative permeability and the extension of Darcy's law for two-phase flow. Viscothermal losses induce the real value static limits of some Willis coupling elements, which appear inconsistent with the fact that Willis coupling should vanish at low frequency in an asymmetric and reciprocal material at first sight. Although counter-intuitive, the response of an asymmetric layered structure converges to that of a symmetric layered structure in the long-wavelength limit despite the presence of non-vanishing Willis coupling parameters. This is a result of Darcy's law and the resulting dynamic effective density in a poroelastic limit where each of the effective parameters couples the properties of the fluid and the solid phases. The existence of two compressional waves further imposes constraints on the value of the effective wavenumber in the fluid phase (the largest of the two wavenumbers), i.e., $\mathrm{Re}(k_e)d \ll 1$. A good indicator for the validity limit of the effective properties is the deviation of α_e from 1 when the two poroelastic layers are saturated by a light fluid. The elements of the Willis coupling tensor cannot be neglected when compared to the first-order homogenization results, notably when the frequency increases. This mostly translates into the fact that the two reflection and absorption coefficients is different. They are correctly calculated when the Willis coupling are accounted for which is not the case when only the first-order homogenization results are used to evaluate the scattering coefficients. The frequency range of validity of these scattering coefficients is, therefore, wider when the Willis coupling matrix is taken into account than in its absence. This work paves the way for the engineering use of Willis materials to control waves in multiphase materials.

ACKNOWLEDGMENTS

M.R.H. was supported in part by the Office of Naval Research under Award N00014-23-1-2660.

AUTHOR DECLARATIONS

Conflict of Interest

The authors have no conflicts to disclose.

Author Contributions

J.-P. Groby: Conceptualization (equal); Formal analysis (equal); Funding acquisition (equal); Investigation (equal); Methodology (equal); Validation (equal); Visualization (equal); Writing – original draft (equal); Writing – review & editing (equal). **M. R. Haberman**: Conceptualization (equal); Formal analysis (equal); Funding acquisition (equal); Investigation (equal); Methodology (equal); Validation (equal); Writing – original draft (equal); Writing – review & editing (equal).

DATA AVAILABILITY

The data that support the findings of this study are available from the corresponding author upon reasonable request.

APPENDIX A: COMPLEX AND FREQUENCY-DEPENDENT DENSITY, BULK MODULUS, AND POROELASTIC PARAMETERS

The complex and frequency dependent density and bulk modulus of the fluid phase, which account, respectively, for the viscous and thermal losses are as follows:[35,36]

$$\tilde{\rho} = \frac{\rho_f \tau_\infty}{\phi}\left(1 + \frac{i\eta\phi}{\omega\kappa_0\rho_f\tau_\infty}\sqrt{1 - i\frac{\omega\rho_f}{\eta}\left(\frac{2\tau_\infty\kappa_0}{\phi\Lambda}\right)^2}\right),$$
$$\tilde{K} = \frac{\gamma P_0}{\phi}\left(\gamma - (\gamma-1)\Big/\left(1 + \frac{i\eta\phi}{\omega\kappa_0'\rho_f \mathrm{Pr}}\sqrt{1 - i\frac{\omega\rho_f \mathrm{Pr}}{\eta}\left(\frac{2\kappa_0'}{\phi\Lambda}\right)^2}\right)\right)^{-1}, \tag{A1}$$

where τ_∞ is the tortuosity; Λ and Λ' are, respectively, the viscous and thermal characteristic lengths; κ_0 and κ_0' are, respectively, the viscous and thermal permeabilities; η is the dynamic viscosity; γ is the heat capacity ratio; and P_0 is the ambient pressure.

The saturation modulus, the additional elastic parameter, and the elastic coupling coefficient are

$$K_G = \frac{K_s - K_b + \phi K_b\left(\frac{K_s}{\phi\tilde{K}} - 1\right)}{1 - \phi - \frac{K_b}{K_s} + \frac{K_s}{\tilde{K}}},$$
$$M = \frac{1}{\frac{\alpha}{K_s} + \phi\left(\frac{1}{\phi\tilde{K}} - \frac{1}{K_s}\right)}, \tag{A2}$$
$$\alpha = 1 - \frac{K_b}{K_s},$$

where K_s and K_b are the bulk moduli of the elastic solid from which the frame is made and of the frame, respectively. The latter equation is usually referred to as the Gassmann equation.[42] When the poroelastic material is saturated by a light fluid such as the air, $K_b/K_s \ll 1$, and these equations reduce to $K_G = K_b + \tilde{K}$, $M = \tilde{K}$, and $\alpha = 1$.

APPENDIX B: MOMENT DENSITY AND CONSTITUTIVE RELATIONS IN ONE-DIMENSIONAL ASYMMETRIC POROELASTIC MEDIUM

Let us divide the state vector $\boldsymbol{W}$ in the one-dimensional asymmetric poroelastic medium as $\boldsymbol{W} = \{\boldsymbol{\sigma}, \boldsymbol{u}\}^T$, with $\boldsymbol{\sigma} = \{\tilde{P}, \sigma_{xx}\}^T$ and $\boldsymbol{u} = \{w, u\}^T$. Equations (4) and (7) then yield the expression,

$$\frac{\partial}{\partial x}\begin{bmatrix}\boldsymbol{\sigma}\\ \boldsymbol{u}\end{bmatrix} = \begin{bmatrix}-i\omega\boldsymbol{\psi}_e & -\omega^2\boldsymbol{\rho}_e\\ \boldsymbol{C}_e & i\omega\boldsymbol{\psi}_e^T\end{bmatrix}\begin{bmatrix}\boldsymbol{\sigma}\\ \boldsymbol{u}\end{bmatrix}. \tag{B1}$$

The bottom two rows of Eq. (B1) then give

$$\boldsymbol{\sigma} = \boldsymbol{C}_e^{-1}\frac{\partial \boldsymbol{u}}{\partial x} - \mathrm{i}\omega \boldsymbol{C}_e^{-1}\boldsymbol{\psi}_e^T\boldsymbol{u} = \boldsymbol{C}_e^{-1}\boldsymbol{\varepsilon} + \boldsymbol{S}_e\boldsymbol{v}, \tag{B2}$$

where $\boldsymbol{\varepsilon} = \partial \boldsymbol{u}/\partial x$ is the normal strain, $\boldsymbol{v} = -\mathrm{i}\omega\boldsymbol{u}$ is the velocity vector, $\boldsymbol{C}_e^{-1}$ is the stiffness matrix, and $\boldsymbol{S}_e = \boldsymbol{C}_e^{-1}\boldsymbol{\psi}_e^T$ is the usual Willis coupling. Introducing the momentum density $\boldsymbol{\pi} = \frac{1}{-\mathrm{i}\omega}\frac{\partial \boldsymbol{\sigma}}{\partial x}$, the first row of Eq. (B1) together with Eq. (B2) becomes

$$\begin{aligned}\boldsymbol{\pi} &= \boldsymbol{\psi}_e\boldsymbol{\sigma} - \mathrm{i}\omega\boldsymbol{\rho}_e\boldsymbol{u}\\ &= \boldsymbol{\psi}_e\boldsymbol{C}_e^{-1}\boldsymbol{\varepsilon} + \boldsymbol{\psi}_e\boldsymbol{S}_e\boldsymbol{v} + \boldsymbol{\rho}_e\boldsymbol{v}\\ &\equiv \tilde{\boldsymbol{S}}_e\boldsymbol{\varepsilon} + \boldsymbol{\rho}_e\boldsymbol{v},\end{aligned} \tag{B3}$$

because $\boldsymbol{\psi}_e\boldsymbol{C}_e^{-1}\boldsymbol{\psi}_e^T$ is a higher-order term and $\tilde{\boldsymbol{S}}_e = \boldsymbol{\psi}_e\boldsymbol{C}_e^{-1} = \boldsymbol{S}_e^T$ because the stiffness matrix is symmetric. This property is a direct result of the causality of the system. Finally, the set of equations describing wave propagation in the asymmetric poroelastic composite takes a similar form as that provided initially in Ref. 1 and reads as

$$\begin{cases}\boldsymbol{\sigma} = \boldsymbol{C}_e^{-1}\boldsymbol{\varepsilon} + \boldsymbol{S}_e\boldsymbol{v},\\ \boldsymbol{\pi} = \boldsymbol{S}_e^T\boldsymbol{\varepsilon} + \boldsymbol{\rho}_e\boldsymbol{v},\end{cases} \tag{B4}$$

where $\boldsymbol{S}_e = \boldsymbol{C}_e^{-1}\boldsymbol{\psi}_e^T$. Note that this form is perfectly equivalent to that provided in Eq. (B1) when taking care of the higher-order terms. We note that one may also define a dynamic density, $\boldsymbol{\rho}_e^{\mathrm{s}} = \rho_e + \boldsymbol{\psi}_e\boldsymbol{C}_e^{-1}\boldsymbol{\psi}_e^T$, that accounts for the higher order effects of Willis coupling. This modified effective density can be understood as representing the effective inertia when the dynamic normal strain is zero. This is analogous to changes in effective stiffness and dielectric permittivity in piezoelectric media under open or short circuit conditions (cf. Auld[43]), which have been shown to influence both dynamic stiffness and density in asymmetric piezoelectric composites known as electromomentum-coupled materials.[12] Note that Pernas–Salomón *et al.*[12] showed that $\boldsymbol{\rho}_e^{\mathrm{s}} \to \boldsymbol{\rho}_e$ while Willis coupling is non-negligible in the long-wavelength limit [see Eq. (41) therein].

APPENDIX C: LOW FREQUENCY LIMIT OF THE COMPLEX AND FREQUENCY DEPENDENT DENSITY AND BULK MODULUS

The low frequency limit of the effective density and compressibility (inverse of the bulk modulus) of the fluid phase are

$$\begin{aligned}\lim_{\omega\to 0}\tilde{\rho} &= \frac{\rho_{\mathrm{f}}\tau_\infty}{\phi}\left(1 + \frac{2\tau_\infty\kappa_0}{\phi\Lambda^2}\right) + \frac{\mathrm{i}\eta}{\omega\kappa_0},\\ \lim_{\omega\to 0}\tilde{C} &= \frac{\phi}{\gamma P_0}\left(\gamma + \frac{\mathrm{i}(\gamma-1)\omega\,\mathrm{Pr}\,\kappa_0'\rho_{\mathrm{f}}}{\eta\phi}\right).\end{aligned} \tag{C1}$$

In the leading order, we have $\lim_{\omega\to 0}\tilde{\rho} \sim \mathrm{i}\eta/\omega k_0$ and $\lim_{\omega\to 0}\tilde{C} \sim \phi/P_0$

APPENDIX D: MOMENT DENSITY AND CONSTITUTIVE RELATION IN ONE-DIMENSIONAL ASYMMETRIC POROELASTIC MEDIUM HAVING A RIGID FRAME

Consider the case where the elastic phase, i.e., the skeleton, is motionless such that $\boldsymbol{\sigma} \equiv -p$ and $\boldsymbol{u} \equiv \phi U = \mathscr{U}$, and therefore, $\boldsymbol{v} \equiv \phi\dot{U} = \mathscr{V}$ is the flow. We then have effective properties given by $\boldsymbol{C}_e \equiv \tilde{C}_e^{\mathrm{ef}}$, $\boldsymbol{\rho}_e \equiv \tilde{\rho}_e^{\mathrm{ef}}$, and $\boldsymbol{\psi}_e \equiv \psi_e^{\mathrm{ef}}$, and Eq. (11) reduces to

$$\begin{cases}-p &= \dfrac{1}{\tilde{C}_e^{\mathrm{ef}}}\dfrac{\partial \mathscr{U}}{\partial x} + \dfrac{\psi_e^{\mathrm{ef}}}{\tilde{C}_e^{\mathrm{ef}}}\mathscr{V},\\ \boldsymbol{\pi} \equiv \dfrac{1}{\mathrm{i}\omega}\dfrac{\partial p}{\partial x} &= \dfrac{\psi_e^{\mathrm{ef}}}{\tilde{C}_e^{\mathrm{ef}}}\dfrac{\partial \mathscr{U}}{\partial x} + \tilde{\rho}_e^{\mathrm{ef}}\mathscr{V}.\end{cases} \tag{D1}$$

Multiplying the first line by $-\mathrm{i}\omega\tilde{C}_e^{\mathrm{ef}}$ and the second line by $\mathrm{i}\omega$ while making use of the first line of Eq. (D1) leads to

$$\begin{cases}\mathrm{i}\omega\tilde{C}_e^{\mathrm{ef}}p = \dfrac{\partial \mathscr{V}}{\partial x} - \mathrm{i}\omega\psi_e^{\mathrm{ef}}\mathscr{V},\\ \dfrac{\partial p}{\partial x} &= \mathrm{i}\omega\dfrac{\psi_e^{\mathrm{ef}}}{\tilde{C}_e^{\mathrm{ef}}}\dfrac{\partial \mathscr{U}}{\partial x} + \mathrm{i}\omega\tilde{\rho}_e^{\mathrm{ef}}\mathscr{V}\\ &= \mathrm{i}\omega\dfrac{\psi_e^{\mathrm{ef}}}{\tilde{C}_e^{\mathrm{ef}}}\left(-\tilde{C}_e^{\mathrm{ef}}p - \psi_e^{\mathrm{ef}}\mathscr{V}\right) + \mathrm{i}\omega\tilde{\rho}_e^{\mathrm{ef}}\mathscr{V}\\ &\equiv -\mathrm{i}\omega\psi_e^{\mathrm{ef}}p + \mathrm{i}\omega\tilde{\rho}_e^{\mathrm{ef}}\mathscr{V},\end{cases} \tag{D2}$$

again because $\left(\psi_e^{\mathrm{ef}}\right)^2/\tilde{C}_e^{\mathrm{ef}}$ is a higher-order term, as noted in Appendix B. The last set of equations can then be rewritten in the form of those describing acoustic wave propagation in a one-dimensional effective fluid with properties that couple pressure and particle velocity due to subwavelength asymmetries,

$$\begin{cases}\dfrac{\partial \mathscr{V}}{\partial x} = \mathrm{i}\omega\psi_e^{\mathrm{ef}}\mathscr{V} + \mathrm{i}\omega C_e^{\mathrm{ef}}p,\\ \dfrac{\partial p}{\partial x} = -\mathrm{i}\omega\psi_e^{\mathrm{ef}}p + \mathrm{i}\omega\tilde{\rho}_e^{\mathrm{ef}}\mathscr{V},\end{cases} \tag{D3}$$

which is identical to Eq. (12).

APPENDIX E: EFFECTIVE PROPERTIES OF A *N*-LAYER LAMELLA

The lamellar system consists of a d-periodic repetition of N layers, as depicted in Fig. 4. The thickness of the n-th layer is l_n, such that $d = \sum_{n=1}^{N} l_n$, and the propagator matrix of this layer is $\boldsymbol{A}_n$. The first two-orders of the BCH formula read as[25]

$$\boldsymbol{A}_e d = \sum_{n=1}^{N}\boldsymbol{A}_n l_n + \sum_{n=N-1}^{1}\frac{1}{2}\left[\sum_{m=N}^{n+1}\boldsymbol{A}_m l_m, \boldsymbol{A}_n l_n\right] + \cdots \tag{E1}$$

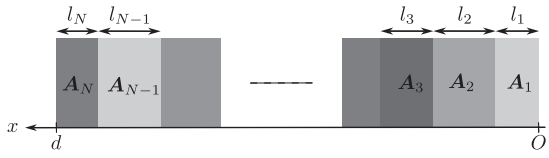

FIG. 4. Sketch of the *N*-layer poroelastic unit-cell.

which provide

$$\boldsymbol{\rho}_e = \sum_{n=1}^{N} \frac{l_n}{d}\boldsymbol{\rho}_n = \begin{bmatrix} \sum_{n=1}^{N} \frac{\tilde{\rho}_n l_n}{d} & \sum_{n=1}^{N} \frac{\rho_{\mathrm{f_n}} l_n}{d} \\ \sum_{n=1}^{N} \frac{\rho_{\mathrm{f_n}} l_n}{d} & \sum_{n=1}^{N} \frac{\rho_n l_n}{d} \end{bmatrix}, \boldsymbol{C}_e = \sum_{n=1}^{N} \frac{l_n}{d}\boldsymbol{C}_n = \begin{bmatrix} \sum_{n=1}^{N} \frac{\tilde{C}_{\mathrm{f_n}} l_n}{d} & \sum_{n=1}^{N} \frac{-\alpha_n \tilde{C}_n l_n}{d} \\ \sum_{n=1}^{N} \frac{-\alpha_n \tilde{C}_n l_n}{d} & \sum_{n=1}^{N} \frac{\tilde{C}_n l_n}{d} \end{bmatrix},$$

$$\begin{aligned}
\chi_e(1,1) &= \frac{\omega^2}{2d} \sum_{n=N-1}^{1} \left(\alpha_n \tilde{C}_n l_n \sum_{m=N}^{n+1} \rho_{\mathrm{f_m}} l_m - \rho_{\mathrm{f_n}} l_n \sum_{m=N}^{n+1} \alpha_m \tilde{C}_m l_m + \tilde{\rho}_n l_n \sum_{m=N}^{n+1} \tilde{C}_{\mathrm{f_m}} l_m - \tilde{C}_{\mathrm{f_n}} l_n \sum_{m=N}^{n+1} \tilde{\rho}_m l_m \right), \\
\chi_e(1,2) &= \frac{\omega^2}{2d} \sum_{n=N-1}^{1} \left(\alpha_n \tilde{C}_n l_n \sum_{m=N}^{n+1} \tilde{\rho}_m l_m - \tilde{\rho}_n l_n \sum_{m=N}^{n+1} \alpha_m \tilde{C}_m l_m + \rho_{\mathrm{f_n}} l_n \sum_{m=N}^{n+1} \tilde{C}_m l_m - \tilde{C}_n l_n \sum_{m=N}^{n+1} \rho_{\mathrm{f_m}} l_m \right), \\
\chi_e(2,1) &= \frac{\omega^2}{2d} \sum_{n=N-1}^{1} \left(\alpha_n \tilde{C}_n l_n \sum_{m=N}^{n+1} \rho_m l_m - \rho_n l_n \sum_{m=N}^{n+1} \alpha_m \tilde{C}_m l_m + \rho_{\mathrm{f_n}} l_n \sum_{m=N}^{n+1} \tilde{C}_{\mathrm{f_m}} l_m - \tilde{C}_{\mathrm{f_n}} l_n \sum_{m=N}^{n+1} \rho_{\mathrm{f_m}} l_m \right), \\
\chi_e(2,2) &= \frac{\omega^2}{2d} \sum_{n=N-1}^{1} \left(\alpha_n \tilde{C}_n l_n \sum_{m=N}^{n+1} \rho_{\mathrm{f_m}} l_m - \rho_{\mathrm{f_n}} l_n \sum_{m=N}^{n+1} \alpha_m \tilde{C}_m l_m + \rho_n l_n \sum_{m=N}^{n+1} \tilde{C}_m l_m - \tilde{C}_n l_n \sum_{m=N}^{n+1} \rho_m l_m \right).
\end{aligned} \tag{E2}$$

APPENDIX F: EVALUATION OF THE SCATTERING COEFFICIENTS OF A POROELASTIC LAMELLA

Assume an asymmetric poroelastic layered medium of length L excited with a normally incident plane wave; see Fig. 1(b). The layered structure is composed of N unit-cells, each composed of two poroelastic layers. The transfer matrix for the unit cell is given in Eq. (3). When excited from the left hand side, the pressure on both sides of the lamella is given by

$$\begin{aligned}
p^+(x) &= e^{-\mathrm{i}k(x-L)} + R^+ e^{\mathrm{i}k(x-L)} \\
p^-(x) &= Te^{-\mathrm{i}kx}.
\end{aligned} \tag{F1}$$

Imposing the boundary conditions, i.e., requiring continuity of pressure, stress, displacement, and relative displacement at the interfaces of both sides of the unit-cell, yields

$$\boldsymbol{W}(L) = \begin{bmatrix} -1 \\ -1 \\ \frac{-\mathrm{i}k}{\omega^2 \rho_{\mathrm{f}}} \\ 0 \end{bmatrix} + \begin{bmatrix} -1 & 0 \\ -1 & 0 \\ \frac{\mathrm{i}k}{\omega^2 \rho_{\mathrm{f}}} & -1 \\ 0 & 1 \end{bmatrix} \begin{bmatrix} R^+ \\ u(L) \end{bmatrix} = \boldsymbol{S}^+ + \boldsymbol{L}^+ \begin{bmatrix} R^+ \\ u(L) \end{bmatrix}, \tag{F2}$$

$$\boldsymbol{W}(0) = \begin{bmatrix} -1 & 0 \\ -1 & 0 \\ \frac{-\mathrm{i}k}{\omega^2 \rho_{\mathrm{f}}} & -1 \\ 0 & 1 \end{bmatrix} \begin{bmatrix} T \\ u(0) \end{bmatrix} = \boldsymbol{L}^- \begin{bmatrix} T \\ u(0) \end{bmatrix},$$

The state vectors at both sides of the lamella are then related via the transfer matrix $\boldsymbol{W}(L) = \left[\exp(\boldsymbol{A}_2 l_2)\exp(\boldsymbol{A}_1 l_1)\right]^N = \boldsymbol{T}_L \boldsymbol{W}(0)$ to give a solution of the system of the form

$$\left[\boldsymbol{T}_L \boldsymbol{L}^- - \boldsymbol{L}^+\right] \begin{bmatrix} R^+ \\ u(0) \\ T \\ u(0) \end{bmatrix} = \boldsymbol{S}^+. \tag{F3}$$

In this latter equation, the left-most quantity is a block matrix of two 4×2 matrices, yielding a 4×4 matrix. Similarly, the state vectors on both sides of the lamella take the following form when excited from the right hand side:

$$\boldsymbol{W}(L) = \begin{bmatrix} -1 & 0 \\ -1 & 0 \\ \frac{\mathrm{i}k}{\omega^2 \rho_{\mathrm{f}}} & -1 \\ 0 & 1 \end{bmatrix} \begin{bmatrix} T \\ u(L) \end{bmatrix} = \boldsymbol{L}'^+ \begin{bmatrix} T \\ u(L) \end{bmatrix}, \tag{F4}$$

$$\boldsymbol{W}(0) = \begin{bmatrix} -1 \\ -1 \\ \frac{\mathrm{i}k}{\omega^2 \rho_{\mathrm{f}}} \\ 0 \end{bmatrix} + \begin{bmatrix} -1 & 0 \\ -1 & 0 \\ \frac{-\mathrm{i}k}{\omega^2 \rho_{\mathrm{f}}} & -1 \\ 0 & 1 \end{bmatrix} \begin{bmatrix} R^- \\ u(0) \end{bmatrix} = \boldsymbol{S}^- + \boldsymbol{L}'^- \begin{bmatrix} T \\ u(0) \end{bmatrix},$$

and the solution to the system reads as

$$\begin{bmatrix} -\boldsymbol{T}_L \boldsymbol{L}'^- & \boldsymbol{L}'^+ \end{bmatrix} \begin{bmatrix} R^- \\ u(0) \\ T \\ u(0) \end{bmatrix} = \boldsymbol{T}_L \boldsymbol{S}^-. \tag{F5}$$

REFERENCES

[1] J. R. Willis, "Variational principles for dynamic problems for inhomogeneous elastic media," Wave Motion **3**, 1–11 (1981).

[2] J. R. Willis, "Variational and related methods for the overall properties of composites," Adv. Appl. Mech. **21**, 1–78 (1981).

[3] J. R. Willis, "The nonlocal influence of density variations in a composite," Int. J. Solids Struct. **21**, 805–817 (1985).

[4] S. Koo, C. Cho, J. Jeong, and N. Park, "Acoustic omni meta-atom for decoupled access to all octants of a wave parameter space," Nat. Commun. **7**, 13012 (2016).

[5] M. B. Muhlestein, C. F. Sieck, P. S. Wilson, and M. R. Haberman, "Experimental evidence of Willis coupling in a one-dimensional effective material element," Nat. Commun. **8**, 15625 (2017).

[6]Y. Liu, Z. Liang, J. Zhu, L. Xia, O. Mondain-Monval, T. Brunet, A. Alù, and J. Li, "Willis metamaterial on a structured beam," Phys. Rev. X **9**, 011040 (2019).
[7]M. B. Muhlestein, C. F. Sieck, A. Alù, and M. R. Haberman, "Reciprocity, passivity and causality in Willis materials," Proc. R. Soc. A **472**, 20160604 (2016).
[8]G. W. Milton, M. Briane, and J. R. Willis, "On cloaking for elasticity and physical equations with a transformation invariant form," New J. Phys. **8**, 248 (2006).
[9]H. Nassar, Q.-C. He, and N. Auffray, "Willis elastodynamic homogenization theory revisited for periodic media," J. Mech. Phys. Solids **77**, 158–178 (2015).
[10]Y. Hao, Y. Shen, J.-P. Groby, and J. Li, "Experimental demonstration of Willis coupling for elastic torsional waves," Wave Motion **112**, 102931 (2022).
[11]L. Quan, D. L. Sounas, and A. Alù, "Nonreciprocal Willis coupling in zero-index moving media," Phys. Rev. Lett. **123**, 064301 (2019).
[12]R. Pernas-Salomón, M. R. Haberman, A. N. Norris, and G. Shmuel, "The electromomentum effect in piezoelectric Willis scatterers," Wave Motion **106**, 102797 (2021).
[13]Y. Meng, Y. Hao, S. Guenneau, S. Wang, and J. Li, "Willis coupling in water waves," New J. Phys. **23**, 073004 (2021).
[14]A. Merkel, V. Romero-García, J.-P. Groby, J. Li, and J. Christensen, "Unidirectional zero sonic reflection in passive PT-symmetric Willis media," Phys. Rev. B **98**, 201102 (2018).
[15]T. Wiest, C. C. Seepersad, and M. R. Haberman, "Robust design of an asymmetrically absorbing willis acoustic metasurface subject to manufacturing-induced dimensional variations," J. Acoust. Soc. Am. **151**, 216–231 (2022).
[16]A. N. Norris and P. Packo, "Non-symmetric flexural wave scattering and one-way extreme absorption," J. Acoust. Soc. Am. **146**, 873–883 (2019).
[17]A. Duval, F. Chevillotte, I. Pereira, S. Futatsugi, and M. L. V. Rodrigues, "Industrial applications of porous media and acoustic metamaterials," in *Acoustic Waves in Periodic Structures, Metamaterials, and Porous Media: From Fundamentals to Industrial Applications*, edited by N. Jimenez, O. Umnova, and J.-P. Groby (Springer, Cham, 2021), pp. 367–440.
[18]Y.-F. Wang, J.-W. Liang, A.-L. Chen, Y.-S. Wang, and V. Laude, "Wave propagation in one-dimensional fluid-saturated porous metamaterials," Phys. Rev. B **99**, 134304 (2019).
[19]P. Leclaire, F. Cohen-Ténoudji, and J. Aguirre-Puente, "Extension of Biot's theory of wave propagation to frozen porous media," J. Acoust. Soc. Am. **96**, 3753–3768 (1994).
[20]J. M. Carcione and G. Seriani, "Wave simulation in frozen porous media," J. Comput. Phys. **170**, 676–695 (2001).
[21]M. A. Biot, "Theory of propagation of elastic waves in a fluid-saturated porous solid. I. Low-frequency range," J. Acoust. Soc. Am. **28**, 168–178 (1956).
[22]M. A. Biot, "Theory of propagation of elastic waves in a fluid-saturated porous solid. II. Higher frequency range," J. Acoust. Soc. Am. **28**, 179–191 (1956).
[23]M. A. Biot, "Mechanics of deformation and acoustic propagation in porous media," J. Appl. Phys. **33**, 1482–1498 (1962).
[24]G. H. Weiss and A. A. Maradudin, "The Baker-Hausdorff formula and a problem in crystal physics," J. Math. Phys. **3**, 771–777 (1962).
[25]Y. Liu, S. Guenneau, and B. Gralak, "Artificial dispersion via high-order homogenization: Magnetoelectric coupling and magnetism from dielectric layers," Proc. R. Soc. A **469**, 20130240 (2013).
[26]M. Malléjac, T. Cavalieri, V. Romero-García, A. Merkel, D. Torrent, J. Christensen, J. Li, and J.-P. Groby, "Non-locality of the Willis coupling in fluid laminates," Wave Motion **110**, 102892 (2022).
[27]J.-P. Groby, M. Malléjac, A. Merkel, V. Romero-García, V. Tournat, D. Torrent, and J. Li, "Analytical modeling of one-dimensional resonant asymmetric and reciprocal acoustic structures as Willis materials," New J. Phys. **23**, 053020 (2021).
[28]L. K. Albarghouty, "On relative permeability: A new approach to two-phase fluid flow in porous media," Master's thesis (Department of Earth, Atmospheric and Planetary Sciences, Massachusetts Institute of Technology, 2017).
[29]D. Lasseux, F. J. Valdés-Parada, J.-F. Thovert, and V. Mourzenko, "Exuding porous media: Deviations from Darcy's law," J. Fluid Mech. **911**, A48 (2021).
[30]M. Sedaghat, S. Azizmohammadi, and S. Matthäi, "Does the symmetry of absolute permeability influence relative permeability tensors in naturally fractured rocks?," J. Petrol. Explor. Prod. Technol. **10**, 455–466 (2020).
[31]J. Cacheux, J. Ordonez-Miranda, A. Bancaud, L. Jalabert, D. Alcaide, M. Nomura, and Y. Matsunaga, "Asymmetry of tensile versus compressive elasticity and permeability contributes to the regulation of exchanges in collagen gels," Sci. Adv. **9**, eadf9775 (2023).
[32]M. E. Rosti, S. Pramanik, L. Brandt, and D. Mitra, "The breakdown of Darcy's law in a soft porous material," Soft Matter **16**, 939–944 (2020).
[33]D. Gedeon, "Dc gas flows in stirling and pulse tube cryocoolers," in *Cryocoolers 9*, edited by R. G. Ross (Springer US, Boston, MA, 1997), pp. 385–392.
[34]P. In 'T Panhuis, S. W. Rienstra, J. Molenaar, and J. J. M. Slot, "Weakly nonlinear thermoacoustics for stacks with slowly varying pore cross-sections," J. Fluid Mech. **618**, 41–70 (2009).
[35]D. L. Johnson, J. Koplik, and R. Dashen, "Theory of dynamic permeability and tortuosity in fluid-saturated porous media," J. Fluid Mech. **176**, 379–402 (1987).
[36]D. Lafarge, P. Lemarinier, J. F. Allard, and V. Tarnow, "Dynamic compressibility of air in porous structures at audible frequencies," J. Acoust. Soc. Am. **102**, 1995–2006 (1997).
[37]J. G. Berryman and G. W. Milton, "Exact results for generalized Gassmann's equations in composite porous media with two constituents," Geophysics **56**, 1950–1960 (1991).
[38]J. G. Berryman, Transversely isotropic poroelasticity arising from thin isotropic layers, in: K. M. Golden, G. R. Grimmett, R. D. James, G. W. Milton, and P. N. Sen (Eds.), *Mathematics of Multiscale Materials* (Springer, New York, 1998), pp. 37–50.
[39]J. G. Berryman, "Effective medium theories for multicomponent poroelastic composites," J. Eng. Mech. **132**, 519–531 (2006).
[40]C. F. Sieck, A. Alù, and M. R. Haberman, "Origins of Willis coupling and acoustic bianisotropy in acoustic metamaterials through source-driven homogenization," Phys. Rev. B **96**, 104303 (2017).
[41]G. Gautier, L. Kelders, J. P. Groby, O. Dazel, L. De Ryck, and P. Leclaire, "Propagation of acoustic waves in a one-dimensional macroscopically inhomogeneous poroelastic material," J. Acoust. Soc. Am. **130**, 1390–1398 (2011).
[42]F. Gassman, "Über die elastizität poröser medien," Vierteljahrsschr. Naturforsch. Ges. Zuerich **96**, 1–23 (1951).
[43]B. Auld, *Acoustic Fields and Waves in Solids* (Wiley, 1973).